Dissociative recombination of BeH^+

J. B. Roos, M. Larsson, and Å. Larson*
Department of Physics, Stockholm University, AlbaNova University Center, S-106 91 Stockholm, Sweden

A. E. Orel
Department of Applied Science, University of California, Davis, California 95616, USA
(Received 1 April 2009; published 6 July 2009)

The cross section for dissociative recombination of BeH^+ is calculated by the solution of the time-dependent Schrödinger equation in the local complex potential approximation. The effects of couplings between resonant states and the Rydberg states converging to the ground state of the ion are studied. The relevant potentials, couplings, and autoionization widths are extracted using *ab initio* electron scattering and structure calculations, followed by a diabatization procedure. The calculated cross sections show a sizable magnitude at low energy, followed by a high-energy peak centered around 1 eV. The electronic couplings between the neutral states induce oscillations in the cross section. Analytical forms for the cross sections at low collision energies are given.

DOI: 10.1103/PhysRevA.80.012501 PACS number(s): 31.50.Df, 34.80.Lx, 31.15.xv, 34.80.Ht

I. INTRODUCTION

The ITER fusion reactor planned for Cadarache, France, is the next major step in fusion research. It is presently scheduled to start its operation in 2016. A critical choice in the construction of ITER is the plasma facing material. There is not a single choice that will fulfill all possible criteria, and research and development is required in order to make an optimal choice. Much effort has been devoted to obtaining reaction cross sections for atoms and molecules present in the edge plasma and the divertor region, not least through the Coordinated Research Projects organized by the International Atomic Energy Agency (IAEA) [1]. Beryllium is a primary choice for the first wall because of its low erosion and atomic number. Even with a low degree of erosion, however, beryllium will enter the plasma, and it is therefore of importance to include surface and volume processes for beryllium in various forms in modeling the edge plasma. Beryllium-containing hydrides will form in the edge plasma, and these molecules will be ionized by electrons. The question posed in this paper is how effectively the BeH^+ ions and its isotopologs are destroyed by electrons. The dominant process destroying BeH^+ in the edge plasma is dissociative recombination. This process has never, as far as we know, been studied experimentally, because of the toxicity of beryllium. Thus, there is a need for theoretical support to determine the cross section for this reaction. In this paper we present the calculation of the dissociative recombination of BeH^+.

The relevant potential curves and autoionization widths are determined using *ab initio* electron-scattering and structure calculations. This is followed by a diabatization procedure, where the electronic couplings between the neutral states can be determined. This is discussed in Sec. II. The nuclear dynamics is then studied using a wave-packet propagation method described in Sec. III. The results are presented in Sec. IV. Atomic units are used throughout the paper unless otherwise stated.

*Corresponding author; aasal@physto.se

II. CALCULATION OF RELEVANT ELECTRONIC STATES

The potential-energy curves of the electronic states relevant for dissociative recombination of BeH^+ are determined by combining structure calculations with electron-scattering calculations. For the structure calculations, the multireference configuration interaction (MRCI) technique is used to determine the neutral electronically bound adiabatic states situated below the potential-energy curve of the ground state ($X\ ^1\Sigma^+$) of the BeH^+ ion.

In a quasidiabatic representation, some of these neutral states will cross the ionic ground state and become resonant states, i.e., they will couple to the ionization continuum and have a finite probability for autoionization. In order to determine the energies and autoionization widths of the resonant states, the complex Kohn variational method [2] is used. In order to obtain the quasidiabatic potentials, the scattering data is combined with a diabatization procedure of the electronically bound states.

Finally, the calculated potential-energy curves, autoionization widths, and electronic couplings between the neutral states can be used in order to carry out calculations on the nuclear dynamics.

A. Structure calculations

The adiabatic potential-energy curve of the BeH^+ ground state ($X\ ^1\Sigma^+$) as well as several excited states of BeH of $^2\Sigma^+$, $^2\Pi$, and $^2\Delta$ symmetries are calculated using the MRCI technique.

For both the structure and scattering calculations, natural orbitals are used. The natural orbitals are determined using MRCI calculations on the BeH^+ ground state. In this calculation, the reference space consists of the $1\sigma, 2\sigma, 3\sigma, 1\pi, 4\sigma$ orbitals, and single and double excitations from the reference configurations into the virtual orbitals are included. The natural orbitals are calculated using a basis set for the H atom of $(4s, 1p)$ contracted to $[3s, 1p]$ [3], while for Be, a basis set of $(10s, 6p, 1d)$ contracted into $[3s, 3p, 1d]$ is used [4,5]. The natural orbitals are then further expanded with

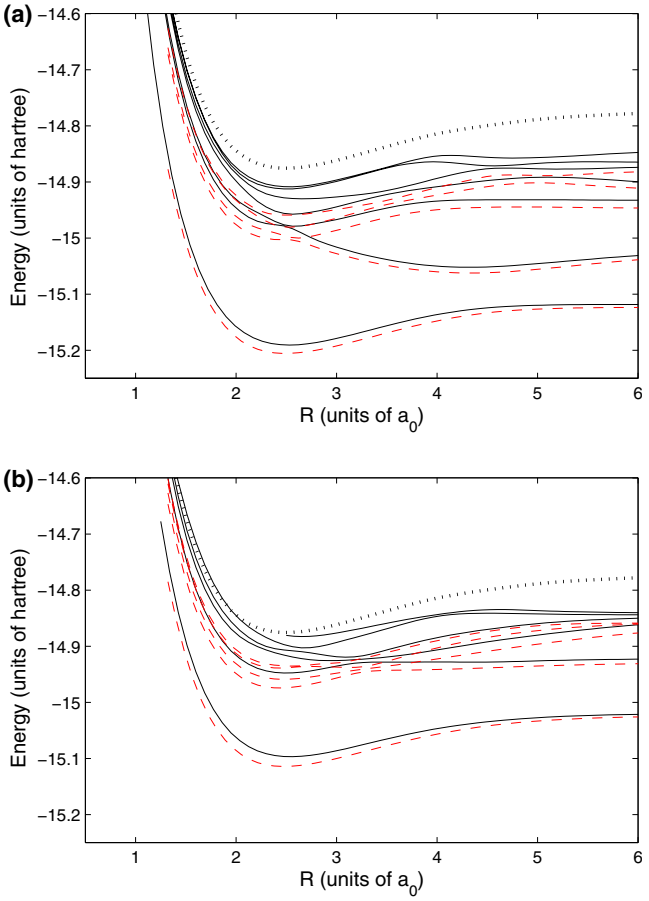

FIG. 1. (Color online) Adiabatic potential-energy curves of BeH of (a) $^2\Sigma^+$ and (b) $^2\Pi$ symmetries. The black dotted curve is the ground state ($X\ ^1\Sigma^+$) of the BeH^+ ion. The black full curves are the potentials calculated here while the dashed (red online) curves are potentials calculated by Pitarch-Ruiz *et al.* [6]

diffuse orbitals in order to accurately describe the Rydberg character of some of the electronic states. The H orbitals are augmented with $(2s,2p,1d)$ orbitals, and the Be orbitals with $(4s,1p,1d)$.

The MRCI calculations on the ionic and neutral excited electronic states are carried out using a reference space consisting of the $1\sigma,2\sigma,3\sigma,1\pi,4\sigma,5\sigma$ orbitals. These natural orbitals all have an occupation number greater than approximately 0.002.

In addition single excitations out of the reference space are included. The calculations are carried out in C_{2v} symmetry. For the neutral system, the MRCI calculations consist of about 5500 configurations in A_1 symmetry, 3700 in A_2, and 4600 in B_1. For all symmetries, the 30 lowest roots are calculated. The potential-energy curves are calculated for internuclear distances in the range $1.0\,a_0 \leqslant R \leqslant 10\,a_0$.

The adiabatic potential-energy curves situated below the ionic ground-state potential are displayed in Fig. 1. In (a) we show the electronic states of BeH of $^2\Sigma^+$ symmetry and in (b) we show the corresponding states of $^2\Pi$ symmetry. The dotted curve is the potential-energy curve of the ionic ground state. The dashed (red online) curves included in the figure are the very accurate potentials of BeH recently calculated by Pitarch-Ruiz *et al.* [6] using a full configuration-interaction calculation with a large basis set. As can be seen in the figure, the potential-energy curves calculated by Pitarch-Ruiz *et al.* are lower in absolute energy. However, our potentials show a similar dependence as a function of the internuclear distance. In the present calculation, our structure calculations are limited by the scattering calculations we perform in the next step (see Sec. II B). In order to describe the resonant and electronically bound states at the same level of theory, it is important to use the same MRCI wave function for the target ion in both the structure and the scattering calculations. In Fig. 1, we do not display any $^2\Delta$ states. Our basis set is not good enough to represent any Rydberg $^2\Delta$ states. We only obtain one resonant state of this symmetry. The higher excited states of $^2\Delta$ symmetry have threshold energies above 1.05 eV relative to the ground vibrational level of the ion and these states will not be important for the total cross section of dissociative recombination at low collision energies.

B. Electron-scattering calculations

By using the complex Kohn variational method [2], the energy positions and autoionization widths of the resonant states are determined. As a target wave function $\mathbf{\Phi}_i(\mathbf{r}_1,\ldots,\mathbf{r}_N)$, the same MRCI wave function for the ion as used in the structure calculations is applied. In the complex Kohn variational method, the $N+1$ electron trial wave function is written as

$$\mathbf{\Psi} = \sum_i A[\mathbf{\Phi}_i(\mathbf{r}_1,\ldots,\mathbf{r}_N)F_i(\mathbf{r}_{N+1})] + \sum_\mu d_\mu \mathbf{\Theta}_\mu(\mathbf{r}_1,\ldots,\mathbf{r}_{N+1}). \tag{1}$$

The first sum is denoted as the P-space portion of the wave function and runs over the energetically open target states. In the case of BeH, only one channel was open. The function $F_i(\mathbf{r}_{N+1})$ is the one-electron wave function describing the scattered electron, and A is an antisymmetrization operator for the electronic coordinates. The second term, denoted as the Q-space portion of the wave function, contains the functions $\mathbf{\Theta}_\mu$, which are square-integrable $N+1$ configuration state functions that are used to describe short-range correlations and the effects of closed channels. The advantage of using natural orbitals is that the orbital space used to generate these states is kept manageably small. The one-electron-scattering wave function F_i is, in the case of electron-ion scattering, further expanded as

$$F_i(\mathbf{r}) = \sum_j c_j^i \phi_j(\mathbf{r}) + [f_l^-(k_i r)\delta_{ll_0}\delta_{mm_0} + T^i_{ll_0mm_0} f_l^+(k_i r)]Y_{lm}(\hat{\mathbf{r}})/r. \tag{2}$$

Here $\phi_j(\mathbf{r})$ are a set of square-integrable functions, $f_l^\pm$ are the outgoing and incoming Coulomb functions, and Y_{lm} are spherical Harmonics. Angular momenta up to $l=6$ and $|m|=4$ are included in the calculation.

By inserting the trial wave function into the complex Kohn functional [2], the unknown coefficients in the trial wave function can be optimized. Then also the T matrix $(T^i_{ll_0mm_0})$ for elastic scattering is obtained, and by fitting the

eigenphase sum of the T matrix to a Breit-Wigner form [7], the energy positions and autoionization widths of the resonant states can be calculated. These electron-scattering calculations are carried out for a fixed geometry of the target ion. For BeH, the five lowest resonant states of $^2\Sigma^+$ and $^2\Pi$ symmetries as well as the lowest resonant state of $^2\Delta$ symmetry are calculated. The electron-scattering calculations are carried out for $1.0a_0 \leq R \leq 3.0a_0$ with steps of $0.25a_0$.

C. Diabatization

For internuclear distances smaller than $5.0a_0$, the electronic ground state of BeH^+ has the dominant configuration $(1\sigma)^2(2\sigma)^2$. All Rydberg states converging to this ionic core have this configuration plus an extra electron in an outer Rydberg-like orbital. The resonant states are in general Rydberg states converging to excited ionic cores. For these states the (2σ) orbital is typically singly occupied. It is therefore relatively easy to use the configuration-interaction coefficients of the MRCI wave functions to follow the resonant states when they cross the Rydberg manifold situated below the ionic ground-state potential. This is done in order to obtain an "estimate" of the quasidiabatic potential-energy curves.

It should be mentioned that, for $R \geq 5.0a_0$, the ionic ground state changes dominant configuration to $(1\sigma)^2(2\sigma)^1(3\sigma)^1$. For these large internuclear distances, the Rydberg states will then have similar configurations as the resonant states and the quasidiabatic potentials are simply estimated by the shape of the adiabatic potentials.

This technique, however, will only provide us with diagonal element of the diabatic potential matrix and not the electronic couplings between the diabatic states. In order to obtain these couplings a diabatization procedure is applied. This diabatization procedure was very recently developed by us for determining the quasidiabatic potential matrix for the HF molecule [8]. There is a unitary transformation matrix $\mathbf{T}$ that will transform the adiabatic potential matrix [with matrix elements $V_{ij}^a = V_i^a(R)\delta_{ij}$] into the diabatic potential matrix

$$\mathbf{V}_d = \mathbf{T}\mathbf{V}_a\mathbf{T}^{-1}. \tag{3}$$

In this diabatization procedure, we assume that the transformation matrix can be written as a product of matrices that describe successive 2×2 rotations among the adiabatic states $\mathbf{T} = \cdots \mathbf{T}_2\mathbf{T}_1$. The matrices $\mathbf{T}_i$ are of the form (in the case of a rotation among states 1 and 2)

$$\mathbf{T}_i = \begin{pmatrix} \cos(\gamma_i) & -\sin(\gamma_i) & 0 & 0 & \cdots \\ \sin(\gamma_i) & \cos(\gamma_i) & 0 & 0 & \cdots \\ 0 & 0 & 1 & 0 & \cdots \\ 0 & 0 & 0 & 1 & \cdots \\ \vdots & \vdots & \vdots & \vdots & \ddots \end{pmatrix}, \tag{4}$$

where we assume that the rotational angles have the analytical form

$$\gamma_i = \frac{\pi}{4}\{1 + \tanh[\alpha_i(R - R_i)]\}. \tag{5}$$

We then perform an optimization procedure, where the unknown parameters α_i and R_i of the rotational angles are determined in order to optimize the agreement between the diagonal elements of the diabatic potential matrix in Eq. (3) and the estimated quasidiabatic potentials obtained using the CI coefficients as described above. When the transformation matrix is optimized, not only the diagonal diabatic potential curves are obtained, but also the electronic couplings between the neutral states. In Fig. 2 we show the diabatic potential curves of BeH obtained using this procedure.

The resonant states situated above the ionic ground state are calculated using the electron-scattering calculations. These resonant states will then cross some of the Rydberg states situated below the ionic potential. Where these curves cross, they will couple by electronic couplings. In Fig. 3, we show examples of the electronic coupling elements between the $^2\Sigma^+$ neutral states marked with thicker curves in Fig. 2 with the other states of the same symmetry. We label the diabatic electronic states from one to n in energy order from lowest to highest at the internuclear distance $1.0a_0$. It should be noted that the electronic couplings are localized to the regions of avoided crossings. The couplings between the electronically bound state 2 and the higher states [see Fig. 3(a)] have the double peak structure since the compact state 2 crosses several of the Rydberg states twice. This state does not, however, cross the ionic ground state. Similar couplings, but now for the $^2\Pi$ manifold, are displayed in Fig. 4.

III. NUCLEAR DYNAMICS

The cross section for dissociative recombination of BeH^+ is calculated by propagating wave packets on the neutral states. The electron capture will induce the initial condition for the wave packets on the resonant state i [9]

$$\Psi_i(t=0,R) = \sqrt{\frac{\Gamma_i(R)}{2\pi}}\chi_v(R). \tag{6}$$

Here Γ_i is the autoionization width for the resonant state and χ_v is the vibrational wave function of the ion. The rotational motion of the molecule is neglected.

The nuclear dynamics is studied by numerically integrating the time-dependent Schrödinger equation,

$$i\frac{\partial}{\partial t}\mathbf{\Psi}(t,R) = -\frac{1}{2\mu}\mathbf{I}\frac{\partial^2}{\partial R^2}\mathbf{\Psi}(t,R) + \mathbf{V}_d\mathbf{\Psi}(t,R), \tag{7}$$

using a Cranck-Nicholson propagator [10]. In the present study, the nuclear dynamics is studied using both coupled and uncoupled electronic states. For the uncoupled states, $\mathbf{V}_d$ is a diagonal matrix with the quasidiabatic potentials of the resonant states on the diagonal. Autoionization is included by letting the resonant states become complex when the resonant state potential is situated above the ionic ground state

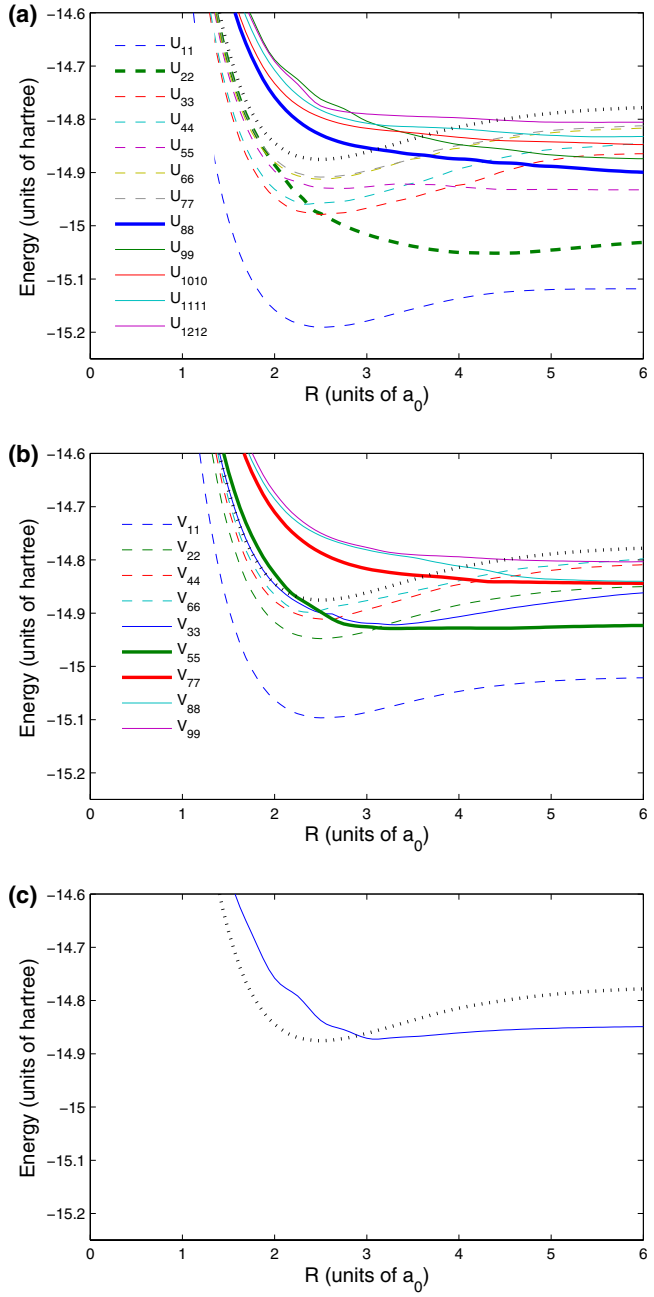

FIG. 2. (Color online) Quasidiabatic potentials of BeH of (a) $^2\Sigma^+$, (b) $^2\Pi$, and (c) $^2\Delta$ symmetries. The solid curves are the resonant states while the electronically bound states are dashed curves. Also the electronic ground state of the BeH^+ is displayed with the dotted curve.

$$\tilde{V}_i^d(R) = V_i^d(R) - i\frac{\Gamma_i(R)}{2}. \tag{8}$$

This is the so-called local approximation for treating autoionization [9]. The validity of this approximation is examined using a nonlocal expression for autoionization [11] and we found that, even for the two lowest resonant states of BeH of $^2\Pi$ symmetry, the local approximation is valid. When the electronic couplings are included, the matrix $\mathbf{V}_d$ in Eq. (7) now contains both the resonant and electronic bound-

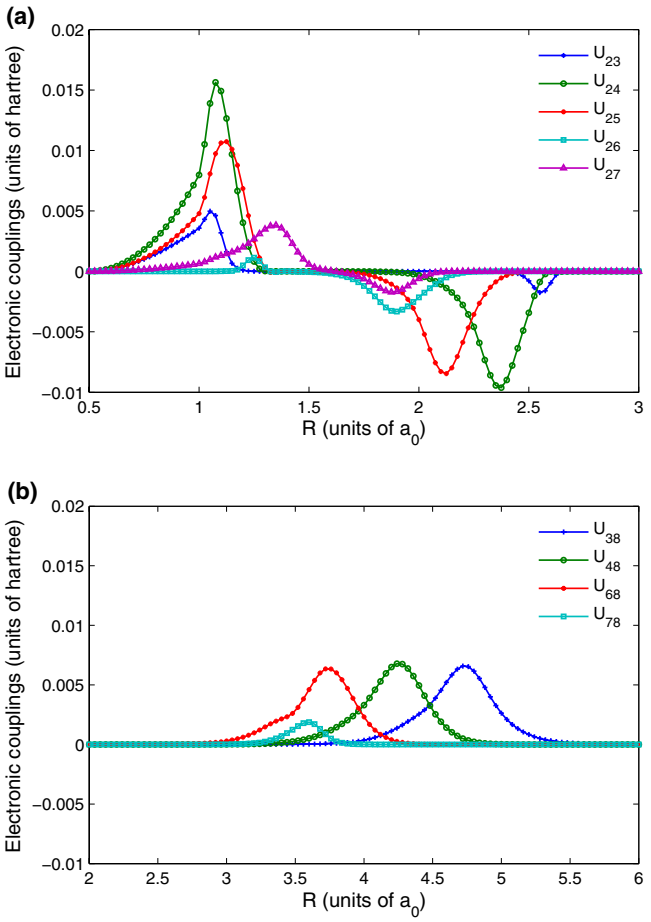

FIG. 3. (Color online) Some of the electronic couplings between diabatic states of $^2\Sigma^+$ symmetry.

state potentials on the diagonal as well as the off-diagonal coupling elements. The electron capture directly into the Rydberg states as well as autoionization out of the Rydberg states are, in the present study, neglected. The neglect of the so-called indirect mechanism is valid when there is a strong direct mechanism [12–14], i.e., when there are resonant states with potentials crossing the ion close to its minimum. The indirect mechanism will only affect the cross section at very low collision energies and create sharp structures in the cross section.

The wave packets are propagated out into the asymptotic region, where the cross section for dissociative recombination is calculated [9,15] by projecting the asymptotic wave packets onto the energy-normalized eigenstates of the fragments

$$\sigma_i(E) = \frac{2\pi^3}{E} g |\langle \Phi_E^i(R) | \Psi_i(t_\infty, R) \rangle|^2. \tag{9}$$

Here g is the ratio of multiplicity between the resonant state and ionization continuum. The total cross section for dissociative recombination is obtained by summarizing all partial cross sections $\sigma(E) = \Sigma_i \sigma_i(E)$.

In the present calculations, the wave packets are propagated on a grid ranging from $0.5a_0$ to $300a_0$ with $dR = 0.01a_0$. The wave packets are propagated with time

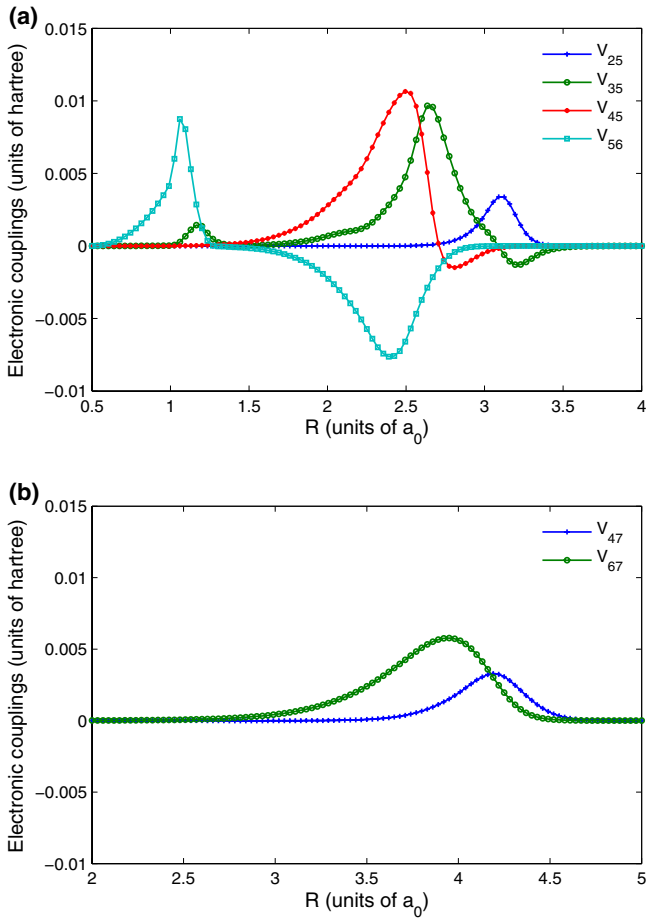

FIG. 4. (Color online) Some of the electronic couplings between diabatic states of $^2\Pi$ symmetry.

steps of $dt=0.1$ a.u. For the uncoupled potentials, the wave packets are propagated until $t_\infty=1000$ a.u., while $t_\infty=4000$ a.u. is needed for the coupled system.

IV. RESULTS AND DISCUSSION

As mentioned above two models are applied in the study of dissociative recombination of BeH^+. In the first model, only the dynamics on the uncoupled resonant states is considered while in the second model the propagation of the wave packets on the coupled potentials is explored. In both models, autoionization from the resonant states is included using local complex potentials.

A. Uncoupled states

As described above, five resonant states of $^2\Sigma^+$ symmetry are included in the model. Only the two lowest resonant states (here labeled with U_{88} and U_{99}) are associated with asymptotic limits that are energetically open at zero collision energy. The following $^2\Sigma^+$ states open up for dissociation at energies of 0.56 eV (U_{1010}), 0.87 eV (U_{1111}), and 1.59 eV (U_{1212}) relative to the ground vibrational level of BeH^+. In the following the cross section for electron recombination with BeH^+ in its ground vibrational state is calculated, that is, the vibrational wave function of the $v=0$ level of BeH^+ is

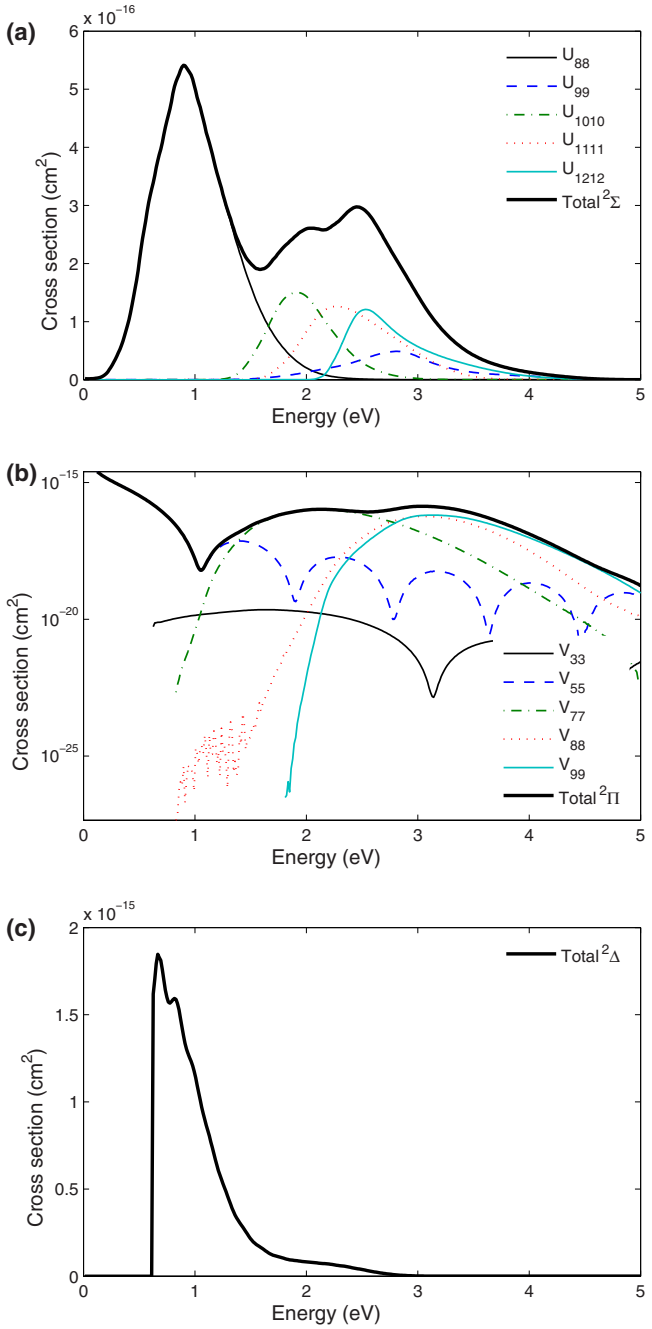

FIG. 5. (Color online) Cross section for dissociative recombination of BeH^+, calculated by propagating wave packets on uncoupled resonant states of (a) $^2\Sigma^+$, (b) $^2\Pi$ (using a linear-log scale), and (c) $^2\Delta$ symmetries. The thin curves are the cross sections originating from each resonant state while the thick curve is the total cross section from the states of a given symmetry.

used in Eq. (6). In Fig. 5(a), we display the cross section for dissociative recombination, obtained when propagating the wave packets on the uncoupled $^2\Sigma^+$ states. As can be seen in the figure, the cross sections originating from all $^2\Sigma^+$ states show a smooth onset. This reflects the fact that the resonant states for this symmetry do not cross the ionic ground-state potential close to the equilibrium separation of the ion. The energy dependence at threshold is therefore determined by the capture probability that is related to the Franck-Condon

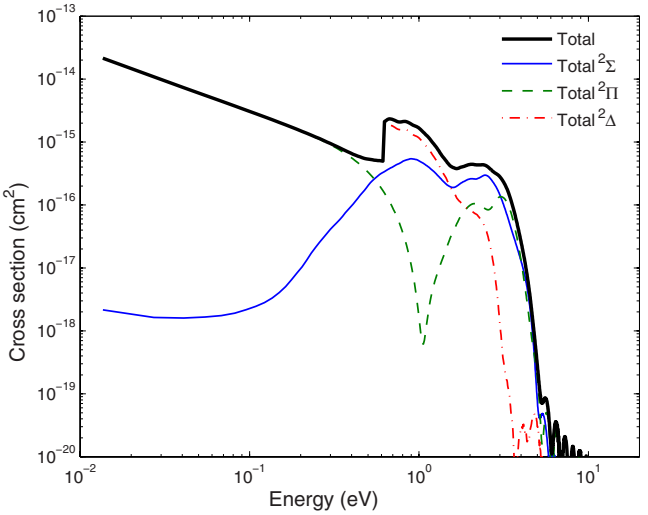

FIG. 6. (Color online) Total cross section for dissociative recombination of BeH^+, calculated using uncoupled resonant states.

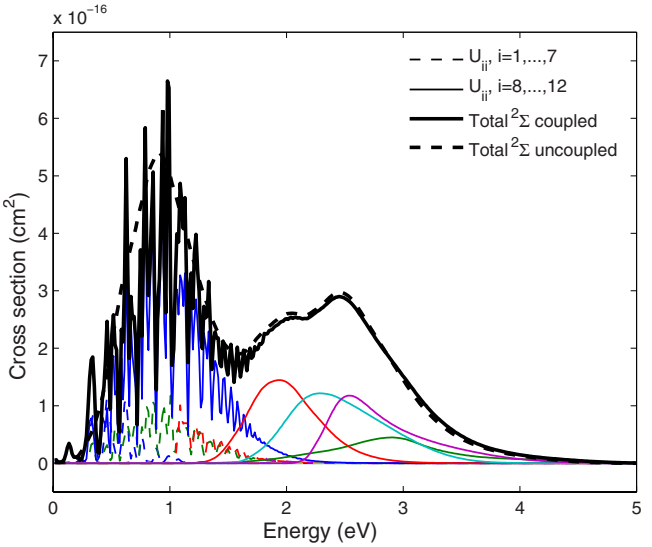

FIG. 7. (Color online) Cross section calculated using the coupled states of BeH of $^2\Sigma^+$ symmetry. The thin solid curves are the cross sections from the resonant states while the dashed curves are cross sections from the electronically bound states. The total cross section originating from the coupled $^2\Sigma^+$ state is shown with the thick black curve. Also the cross section calculated using uncoupled $^2\Sigma^+$ states is displayed with a thick dashed black curve.

factors between the initial vibrational wave function of the ion and the continuum wave function of the resonant states.

The situation is different for the resonant states of $^2\Pi$ symmetry, where two states (labeled with V_{33} and V_{55}) cross the ion potential at smaller distances than the equilibrium distance. The first resonant state (V_{33}) has a threshold of about 0.63 eV while the second state (V_{55}) is energetically open for dissociation at zero collision energy. The cross section from this state shows the typical $1/E$ dependence [16] of the cross section at low energies. The remaining states of $^2\Pi$ symmetry have threshold energies of about 0.83 (for V_{77} and V_{88}) and 1.81 eV for V_{99}. As can be seen in Fig. 5(b), where the cross section from the $^2\Pi$ states are plotted using a linear-log scale, it is the low-energy tail of the cross section from the second resonant state (V_{55}) that dominates the low-energy cross section for this symmetry.

Finally, in Fig. 5(c), the cross section from the $^2\Delta$ resonant state is displayed. This state opens up for dissociation at 0.63 eV and the cross section shows a sharp threshold at this energy.

In Fig. 6, the total cross section using a log-log scale calculated with uncoupled resonant states is shown. In Fig. 6, also the contribution to the cross section from states of the different symmetries is displayed. As can be seen, at low energy the cross section is dominated by resonant states of $^2\Pi$ symmetry. The sharp threshold around 0.63 eV, arising from the $^2\Delta$ resonant state, can be seen in the total cross section.

B. Coupled states

As mentioned above, several resonant states of BeH are not energetically open for dissociation at zero collision energy. We therefore wish to examine a model where the electronic couplings between the resonant and electronically bound states are included. We have previously seen for other systems such as HF^+ [8,17] that the inclusion of electronic couplings between the neutral states may open up pathways to dissociation. Flux that, in the uncoupled model, is trapped in bound potentials will transfer to lower states that are open for dissociation.

As described above in Sec. II C, the neutral states are diabatized and the electronic couplings are determined. For the states of $^2\Sigma^+$ symmetry, seven states are diabatized, i.e., the lowest resonant state and six electronically bound states. In a quasidiabatic representation, there is one compact electronically bound state that will cross several of the Rydberg states situated below the ionic ground state. However, this state will never cross the ion potential and become a resonant state. The ground state of BeH, $X\,^2\Sigma^+$, is assumed not to couple to the higher electronic states. Due to numerical limitations in the optimization procedure, the electronic couplings to the higher resonant states of this symmetry are not calculated. The wave packets are then propagated using the full diabatic potential matrix. In Fig. 7, the cross section, calculated using the coupled $^2\Sigma^+$ states, is shown. In Fig. 7, also the cross section calculated using uncoupled states are displayed.

The inclusion of the electronic couplings will not dramatically change the magnitude of the cross section. Sharp structure is created both in the partial cross sections as well as in the total cross section. This structure can be interpreted as Feshbach resonances created when the states open for dissociation are coupled to the nuclear bound states. Structures in the cross section are then formed when the wave packets couple from a resonant state and form a vibrationally bound state in another potential. Similar structures were seen in the cross section of HF^+ [8]. Above the dissociation energy of the ion (around 2.66 eV), there are no bound vibrational levels of the Rydberg states and this explains the lack of structures at higher energies. Furthermore, the dynamics on the highest $^2\Sigma^+$ resonant states is studied using uncoupled potentials.

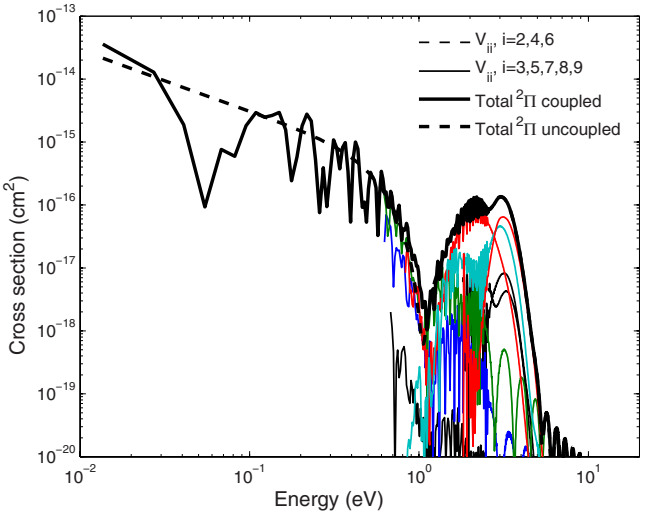

FIG. 8. (Color online) Cross section calculated using the coupled states of BeH of $^2\Pi$ symmetry. Also the cross section calculated using uncoupled resonant states is displayed.

When the electronic states of $^2\Pi$ symmetry are diabatized, eight states are included, i.e., all five resonant states and three electronically bound states. The lowest $A\ ^2\Pi$ state is not included in the process. Again, the electronic couplings induce sharp oscillations in the cross sections but they will not significantly affect the magnitude of the cross section as can be seen in Fig. 8.

The fact that the inclusion of the couplings does not increase the magnitude of the cross section at low energies may be understood by smooth onset of most of the calculated partial cross sections. Hence, it is the electron capture that limits the energy components of the wave packets captured into the resonant states. Simply, there is no low-energy components initiated in the resonant states that can find a way to dissociate by inclusion of electronic couplings.

Figure 9 shows the total cross section for dissociative recombination of BeH^+ calculated using both the uncoupled and coupled models. Both models produce a cross section with a similar magnitude but oscillations are created when the electronic couplings are included. The cross section has a low-energy $1/E$ dependence and a magnitude of about 3×10^{-14} cm^2 at $E=0.01$ eV. This is a typical magnitude for a dissociative recombination cross section of a diatomic molecule [18]. Furthermore, the cross section shows a high-energy peak centered around 1 eV. Similar high-energy peaks were seen in the cross section for dissociative recombination for several ionic species [18]. The sharp threshold around 0.63 eV in the total cross section comes from the $^2\Delta$ resonant state.

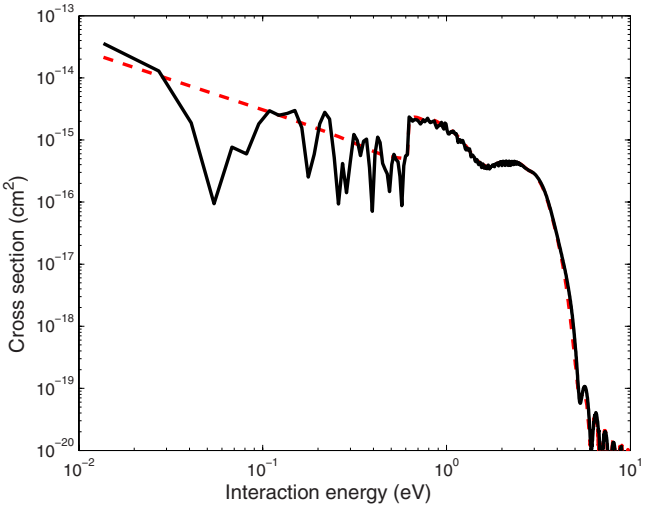

FIG. 9. (Color online) Total cross section for dissociative recombination of BeH^+, calculated using coupled and uncoupled potentials.

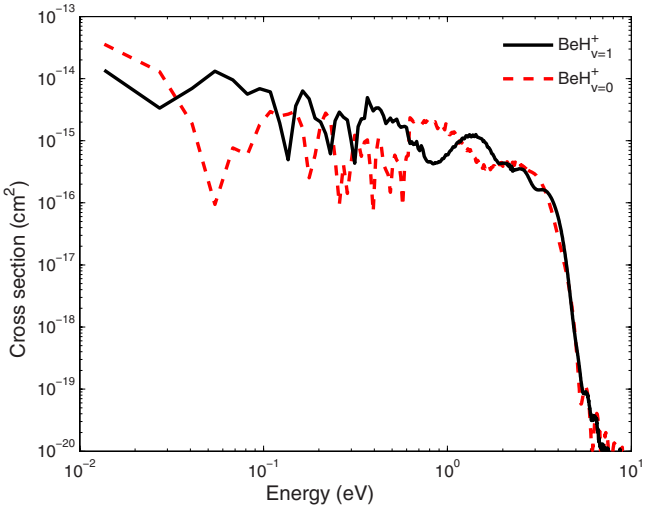

FIG. 10. (Color online) Total cross section for dissociative recombination of BeH^+ in the $v=1$ and $v=1$ vibrational states.

C. Effects of vibration

The cross section for dissociative recombination with BeH^+ in the $v=1$ vibrational level is calculated using the $\chi_{v=1}$ vibrational wave function in the initial condition of the wave packets [Eq. (6)]. Furthermore, the energy scale is shifted to account for the shift in energy of the target ion. The wave packets are then propagated on the coupled potentials. In Fig. 10, we compare the total cross section for dissociative recombination of BeH^+ in $v=0$ and $v=1$. It can be seen that the shift in the energy scale causes shifts of the resonant structures as well as the high-energy peak toward smaller energies. Furthermore, the cross section at low collision energies is increased and this can be understood by larger capture probability into the low lying resonant state for the vibrationally excited ion.

D. Effects from isotopic substitution

The cross section for dissociative recombination with BeD^+ in the $v=0$ vibrational state is calculated by using the same set of potentials, widths, and couplings, but changing the reduced mass to the mass of BeD. Both when the vibrational wave function of the target ion is calculated as well as in the wave-packet propagation, the mass has to be changed. Again, the coupled potentials are used for calculating the

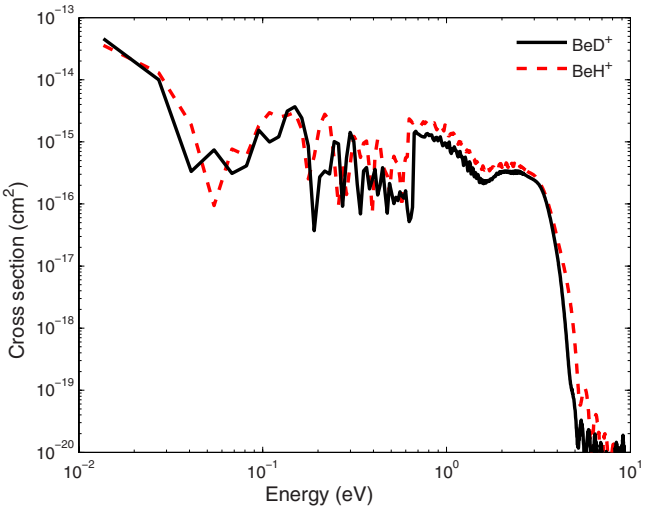

FIG. 11. (Color online) Total cross section for dissociative recombination of BeD^+ and BeH^+ in their lowest $v=0$ vibrational states.

cross section. The resulting cross section is displayed in Fig. 11 and compared with the corresponding cross section for BeH^+. The cross section for the two isotopologs are similar in shape and magnitude. They both show oscillations induced by the electronic couplings as well as the high-energy peak around 1 eV. The magnitude of the high-energy peak is smaller for the heavier isotopolog and similar behaviors have been seen for the high-energy peak observed in, for example, dissociative recombination with H_3^+ [19]. The cross section for electron recombination with BeD^+ in the vibrationally excited $v=1$ state is calculated and is similar to BeH^+, the positions of the structures in the cross section as well as the high-energy peak are shifted in the energy, and the magnitude of the low-energy cross section is increased.

E. Analytical forms for the cross sections

To simplify the use of the calculated cross sections in modeling of the fusion plasmas, the cross sections have been fitted to analytical forms. The cross sections calculated using uncoupled potentials have been used for the fitting. These cross sections show a smooth energy dependence at collision energies below about 0.3 eV that easily can be fitted to functions of the form

$$\sigma(E) = \frac{\sigma_0}{E^b}. \tag{10}$$

In Table I, the values of the parameters σ_0 and b are given for the fits of the calculated cross sections for dissociative recombination of BeH^+ and BeD^+ in the $v=0$ and $v=1$ vibrational levels.

TABLE I. Parameters for the fitted form of the dissociative recombination cross sections at low collision energies.

Ion	Vibrational level	σ_0 (10^{-16}cm^2 eV^b)	b
BeH^+	$v=0$	3.10	0.99
BeH^+	$v=1$	6.90	0.93
BeD^+	$v=0$	3.32	1.02
BeD^+	$v=1$	4.72	1.05

V. CONCLUSIONS

The cross section for dissociative recombination of BeH^+ has been calculated. This cross section is important in the modeling of the fusion plasmas. However, the toxicity of BeH^+ makes measurements on the reaction extremely difficult. In the present study, structure and electron-scattering calculations are combined to obtain quasidiabatic potentials of BeH. Using an optimization procedure, the electronic couplings between the resonant states are estimated. The dynamics of the reaction is then explored using a wave-packet technique. The reaction is studied assuming both uncoupled and coupled potentials. The inclusion of the couplings causes oscillations in the cross section and will not significantly affect the magnitude of the cross section. The cross section shows a low-energy $1/E$ dependence followed by a high-energy peak centered around 1 eV. The cross section for dissociative recombination with vibrationally excited $v=1$ ions is larger at low collision energies than the corresponding cross section for vibrationally relaxed ions. The cross section for the heavier isotopolog BeD^+ is similar to the cross section for BeH^+, except for the high-energy peak that becomes smaller in magnitude.

ACKNOWLEDGMENTS

We are thankful for the data of the calculated potential curves sent to us by Jose Sanchez-Marin. Å.L. acknowledges support from The Swedish Research Council and A.E.O. acknowledges support from the National Science Foundation, Grant No. PHY-05-55401. M.L. participated in the IAEA Coordinated Research Project "Atomic and Molecular Data for Plasma Modelling."

[1] IAEA Report No. INDC(NDS)-0491, 2006 (unpublished).
[2] T. N. Rescigno, C. W. McCurdy, A. E. Orel, and B. H. Lengsfield III, *The Complex Kohn Variational Method in Computational Methods for Electron-Molecule Scattering*, edited by W. H. Huo and F. A. Gianturco (Plenum, New York, 1995).
[3] T. H. Dunning, Jr., J. Chem. Phys. **53**, 2823 (1970).
[4] T. H. Dunning, Jr. and P. J. Hay, *Methods of Electronic Structure Theory*, edited by H. F. Schaefer III (Plenum Press, New York, 1977).
[5] D. Feller, J. Comput. Chem. **17**, 1571 (1996).

[6] J. Pitarch-Ruiz, J. Sánchez-Marin, A. M. Velasco, and I. Martin, J. Chem. Phys. **129**, 054310 (2008).
[7] S. Geltman, *Topics in Atomic Collision Theory* (Academic Press, New York, 1997), p. 31.
[8] J. B. Roos, A. E. Orel, and Å. Larson, Phys. Rev. A **79**, 062510 (2009).
[9] C. W. McCurdy and J. L. Turner, J. Chem. Phys. **78**, 6773 (1983).
[10] A. Goldberg, H. M. Schey, and J. L. Schwartz, Am. J. Phys. **35**, 177 (1967).
[11] A. Giusti-Suzor, J. N. Bardsley, and C. Derkits, Phys. Rev. A **28**, 682 (1983).
[12] D. R. Bates, J. Phys. B **24**, 695 (1991).
[13] A. I. Florescu, V. Ngassam, I. F. Schneider, and A. Suzor-Weiner, J. Phys. B **36**, 1205 (2003).
[14] V. Ngassam and A. E. Orel, Phys. Rev. A **73**, 032720 (2006).
[15] K. C. Kulander and E. J. Heller, J. Chem. Phys. **69**, 2439 (1978).
[16] E. P. Wigner, Phys. Rev. **73**, 1002 (1948).
[17] J. B. Roos, Å. Larson, and A. E. Orel, Phys. Rev. A **78**, 022508 (2008).
[18] A. Al-Khalili *et al.*, Phys. Rev. A **68**, 042702 (2003).
[19] M. Larsson, H. Danared, Å. Larson, A. Le Padellec, J. R. Peterson, S. Rosen, J. Semaniak, and C. Strömholm, Phys. Rev. Lett. **79**, 395 (1997).